

PAPER

The energy structure and decay channels of the $4p^6$ -shell excited states in Sr



To cite this article: A Kupliauskien *et al* 2017 *J. Phys. B: At. Mol. Opt. Phys.* **50** 225201

View the [article online](#) for updates and enhancements.

Related content

- [The 5p autoionization spectra of Ba atoms excited by electron impact: identification of lines](#)
V Hrytsko, G Kereviius, A Kupliauskien *et al.*
- [Electron and photon impact excitation of inner shells in alkali atoms](#)
A Borovik, O Zatsarinny and K Bartschat
- [The 4 p6 autoionization cross section of Rb atoms excited by low-energy electron impact](#)
A Borovik, V Roman and A Kupliauskien

The energy structure and decay channels of the $4p^6$ -shell excited states in Sr

A Kupliauskienė¹ , G Kerevičius¹, V Borovik^{2,4}, I Shafranyosh² and A Borovik^{2,3} 

¹Institute of Theoretical Physics and Astronomy, Vilnius University, Vilnius, LT-10257, Lithuania

²Uzhgorod National University, Uzhgorod, 88000, Ukraine

³Institute of Electron Physics, Uzhgorod, 88017, Ukraine

E-mail: alicija.kupliauskiene@tfai.vu.lt and baa1948@gmail.com

Received 13 April 2017, revised 7 September 2017

Accepted for publication 4 October 2017

Published 30 October 2017



CrossMark

Abstract

The ejected-electron spectra arising from the decay of the $4p^5nl'n''l'''$ autoionizing states in Sr atoms have been studied precisely at the incident-electron energies close to excitation and ionization thresholds of the $4p^6$ subshell. The excitation behaviors for 58 lines observed between 12 and 21 eV ejected-electron kinetic energy have been investigated. Also, the *ab initio* calculations of excitation energies, autoionization probabilities and electron-impact excitation cross sections of the states $4p^5nl'n''l'''$ ($nl = 4d, 5s, 5p; n'l' = 4d, 5s, 5p; n''l'' = 5s, 6s, 7s, 8s, 9s, 5p, 6p, 5d, 6d, 7d, 8d, 4f, 5g$) have been performed by employing the large-scale configuration-interaction method in the basis of the solutions of Dirac–Fock–Slater equations. The obtained experimental and theoretical data have been used for the accurate identification of the 60 lines in ejected-electron spectra and the 68 lines observed earlier in photoabsorption spectra. The excitation and decay processes for 105 classified states in the $4p^55s^2nl$, $4p^54d^2nl$ and $4p^55snl'n''l'''$ configurations have been considered in detail. In particular, most of the states lying below the ionization threshold of the $4p^6$ subshell at 26.92 eV possess up to four decay channels with formation of Sr^+ in $5s_{1/2}$, $4d_{3/2,5/2}$ and $5p_{1/2,3/2}$ states. Two-step autoionization and two-electron Auger transitions with formation of Sr^{2+} in the $4p^6\ ^1S_0$ ground state are the main decay paths for high-lying autoionizing states. The excitation threshold of the $4p^6$ subshell in Sr has been established at 20.98 ± 0.05 eV.

Keywords: atom, ion, autoionization, ejected-electron spectra

(Some figures may appear in colour only in the online journal)

1. Introduction

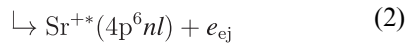
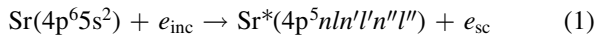
The spectrometry of scattered and ejected electrons is known as the most efficient experimental method to investigate the autoionizing phenomena in processes of electron-impact excitation/ionization of atoms. Data on the energy structure, excitation cross sections, and decay channels of autoionization states (AIS), if obtained at low impact energies, provide unique information on electron–core or electron–electron correlations in many-electron atomic systems. These data, therefore, serve as a good basis for more sophisticated contemporary studies using ultrashort photon beams [1, 2].

Strontium as a divalence atomic system with high polarizability is widely used in cooling and trapping techniques to solve a number of fundamental physical and technical tasks, including implementation of optical lattice clocks [3], quantum information processing [4], studying the properties of ultracold plasma [2, 5]. The energy spectrum of Sr atoms plays an important role in the development of the theory of complex atomic spectra. However, despite this importance, available information on the energy structure of Sr atoms is limited to data for levels arising from excitation of the $5s^2$ valence shell and located below the $4p^64d_{3/2,5/2}$ ionization limits [6].

The electron excitation of the $4p^6$ subvalence subshell in Sr leads to the formation of the $4p^5nl'n''l'''$ states for which

⁴ Author to whom all correspondence should be addressed.

the processes of excitation and subsequent radiationless decay can be described by the following reactions



Both processes have been the subject of experimental and theoretical investigations since the 1970s. Particularly, the energy structure of dipole-allowed states (with the total angular momentum $J = 1$) in the $4p^55s^24d$, $6s$, $4p^54d^25s$, $4d$ and $4p^55p^24d$, $5s$ odd configurations has been established from the high-resolution photoabsorption studies [7–9]. Most of the observed lines were ordered into 13 Rydberg series while those not included in the series were identified by comparison with quasi-relativistic multiconfiguration Hartree–Fock calculations [8]. Authors noted broad agreement between calculations and observations only at wavelengths greater than 495 Å.

The radiationless decay of the $4p^6$ subshell excited states in strontium has been first studied by measuring the ejected-electron spectrum at 90° to an incident-electron beam of 2 keV [10]. The strongest among the 34 lines observed between 10.3 and 20.9 eV ejected-electron energy have been attributed to the decay of the $4p^5nl'n''l'''$ ionic AIS. Only one line at 19.59 eV has been identified as associated with the decay of the $4p^54d5s^2\ ^1P_1$ atomic state.

In order to distinguish the $4p^6$ excitation and ionization processes in Sr, the ejected-electron spectra have been measured in a broad incident-electron energy range, i.e. from 23.5 to 500 eV [11], from 45 to 1500 eV [12] and from 21 to 200 eV [13]. In accordance with the different excitation thresholds and excitation dynamics, the observed lines have been arranged into two main groups associated with the decay of atomic $4p^5nl'n''l'''$ and ionic $4p^5nl'n''l'''$ AIS [11, 12]. Within the first group, the lines with the highest intensity at low/high impact energies have been associated, respectively, with the decay of dipole forbidden/allowed AIS. The simultaneous appearance of atomic lines in spectra has been ascribed to multichannel decay of some atomic AIS. Up to five decay channels with formation of Sr^+ in $4p^6nl$ excited states have been reported [13]. Thus, the main causes of the complex structure of the electronic spectra have been identified in these studies. On the other hand, the poor incident-electron energy resolution (FWHM ≥ 0.5 eV), the large increment step of the impact energy and different observation angles (75° [11] and 90° [12, 13]) resulted in an essential difference of the obtained data on the number of lines observed in spectra, on their excitation thresholds and excitation behaviors. Under these conditions, all efforts to perform a more or less reliable identification of lines failed [12, 14]. As the authors stated, the proposed assignments can be considered as reliable only for six ejected-electron lines arising from the decay of the $4p^54d5s^2\ ^3P_{0,1,2}$ and $^3F_{2,3,4}$ most low-lying atomic AIS.

Meanwhile, according to our previous analysis of ejected-electron spectra of heavy rubidium [15], caesium [16] and

barium [17] atoms, the sufficiently complete and accurate identification of lines is possible provided that (i) the accurate experimental data on excitation energies and excitation behaviors of ejected-electron lines are available and (ii) in calculations, the relativistic and correlation effects are properly taken into account.

The present work is a continuation of our investigations into the energy structure, decay channels and excitation dynamics of the outer p^6 subshell excited atomic AIS in alkaline and alkaline earth elements (see e.g. [17] and references therein). In order to evaluate the excitation thresholds and decay channels of the atomic AIS in Sr, we have studied the intensity behavior of ejected-electron spectra in a broad electron-impact energy range starting from the appearance of the first spectral line up to 102 eV. Unlike in previous studies, we investigated the entire ejected-electron energy range 12–21 eV where the lines arising from the decay of atomic AIS can be observed. The data obtained close to excitation and ionization thresholds of the $4p^6$ subshell have enabled us to distinguish the lines arising from the decay of atomic and ionic AIS, of dipole-allowed and dipole-forbidden atomic AIS and, thus, to establish the decay channels of atomic AIS. Basing on *ab initio* calculations of energies, decay rates and excitation cross sections of the $4p^5nl'n''l'''$ states by employing the standard software package flexible atomic code (FAC) [18], 60 lines in ejected-electron spectra [10, 11, 13] and 68 lines in photoabsorption spectra [7–9] were classified/re-classified as attributed to the excitation and subsequent radiationless multichannel decay of 105 atomic states predominantly from $4p^55s^2nl$, $4p^54d^2nl$ and $4p^54d5snl$ configurations. In section 2, we briefly describe the apparatus and the measurement procedure. In section 3, the calculation method is described. In section 4, the results of the measurements and calculations are considered. In section 5, the excitation and decay processes of the classified states are discussed based on the performed identification of lines and other available data. Conclusions are drawn in section 6.

2. Experiment

The crossed-beam ejected-electron spectrometer and the measurement procedure used in the present work were described in detail in our previous publications [17, 19]. Briefly, an energy-selected electron beam from a 127° cylindrical monochromator was focused onto a vapor beam produced by a resistively heated oven. The latter was operated at a typical temperature of 550°C . The beam density in the interaction region was approximately 1×10^{11} atoms cm^{-3} [20]. The scattered and ejected electrons were detected by the 127° electron energy analyzer with an angular resolution of $\pm 2^\circ$ positioned at a 'magic' angle of 54.7° to the incident-electron beam (for details, see section 3). The incident and ejected-electron energy resolutions (FWHM) were about 0.1 eV and 0.07 eV, respectively.

The previous studies of ejected-electron [11] and photoionization [21] spectra of Sr atoms have determined the ionization threshold of the $4p^6$ subshell as the excitation energy of the lowest ionic AIS ($4p^5 4d 5s$) $^4P_{1/2}$ at 26.92 ± 0.01 eV. As regards the excitation threshold of the $4p^6$ subshell, the present calculations show that its value is determined by the excitation energy of the ($4p^5 4d 5s^2$) 3P_0 lowest dipole-forbidden atomic AIS at 20.961 eV (see table 1). Because the excitation energy of the nearest dipole-allowed state 3P_1 is known at 21.099 eV [8], one may conclude that the 3P_0 state and, therefore, the excitation threshold of the $4p^6$ subshell in Sr must lie below 21 eV. This implies that the lines arising from the decay of the 3P_0 state must be the first which appear in ejected-electron spectra at low impact energies.

To establish the order of appearance of lines in the spectra and, therefore, to determine their excitation thresholds, the spectra were measured in series, step-by-step for different incident-electron energy values over the range from 20.8 eV up to 102 eV. The smallest increment step of the incident energy was 0.1 eV. To control the stability of experimental conditions, a 'test' spectrum containing both ejected-electron and energy-loss lines was measured before and after each set of three main ejected-electron spectra (see spectrum at 21.49 eV in figure 1). The energy scales were calibrated by comparing the relative position of the $4p^6 5s 6s$ 1S_0 energy-loss line 1' at 3.793 eV [6] and the ejected-electron line 43 at 15.43 eV which corresponds to the decay of the 3P_1 lowest dipole-allowed AIS at 21.099 eV ($\lambda = 587.565$ Å) [8]. The uncertainties of the incident-electron and ejected-electron energy scales were about ± 0.07 eV and ± 0.05 eV, respectively.

All measured spectra were processed for subtracting the background intensity and for deriving the energy positions of lines. The symmetrical Gaussian function was used in the fitting procedure because no evidence of interference [22] or post-collision interaction [23] effects was seen in the ejected-electron spectra at low impact energies. The data on energy positions of lines were determined as average values taken from three to five spectra and have an estimated uncertainty of ± 0.05 eV.

3. Method of calculations

The calculations of energies, autoionization probabilities, oscillator strengths of electric dipole transitions, and electron-impact excitation cross sections were performed in the basis of mixed relativistic configurations by using FAC computer code [18]. The radial orbitals for the construction of the basis state wave functions were derived from a modified self-consistent Dirac–Fock–Slater iteration on a fictitious mean configuration with fractional occupation numbers representing an average electron cloud of all configurations included in the calculation.

In order to optimize the local central potential including the approximated exchange part, the following singly excited configurations $4p^6 5s nl$ ($nl = 4d, 5d, 6d, 6s, 5p, 6p, 4f, 5f$)

were used. The ground, singly excited configurations $4p^6 5s nl$ ($nl = 5s, \dots, 10s; 5p, \dots, 10p; 4f, \dots, 7f; 5g, \dots, 7g$) and $4p$ -core excited $4p^5 [4d(4d, 4f, 5s-5g, 6s, 6p)nl; 4f(4f, 5s, 5p, 5d, 5g, 6s)nl; 5s(5s-5g, 6s-6f, 7s, 7p, 7d)nl; 5p(5p-5g, 6s, 6p)nl]$ configurations were used to take into account the correlation effects. Since local potential was optimized only for the singly excited configurations, the following correction procedure was applied to reduce the errors on total energies. Before the potential for the mean configuration with fractional occupation numbers was calculated, the optimized potential and corresponding average energy for each configuration was obtained. Then, the average energy for each configuration was calculated with the potential optimized for the mean configuration with fractional occupation numbers. The difference of two average energies was applied as a correction to the states within each configuration after the Hamiltonian was diagonalized. The total number of both odd and even states included in the calculation was 29824. The same basis set was used to calculate electron-impact excitation cross sections.

For the calculation of autoionization probabilities, the basis set of Sr was supplemented with the configurations $4p^6 nl$ ($nl = 5s, 6s, 5p, 6p, 4d, 5d, 4f$) of Sr^+ to include the most important Auger decay channels. The configurations $4p^5 5s^2, 4p^5 4d^2$ and $4p^5 4d 5s$ of Sr^+ were also included to take into account additional decay channels which are energetically allowed for the atomic AIS with excitation energies greater than 27 eV. The autoionization probabilities were calculated in the relativistic distorted-wave and the isolated resonance approximations. The local central potential was the same to that used in the calculations of energies and excitation cross sections of Sr. The excitation cross sections were calculated in the relativistic distorted-wave approximation [18].

The energy levels calculated with FAC code [18] were described by using quantum numbers jjJ of the relativistic coupling scheme of angular momenta. The obtained expansion coefficients were transformed to the LSJ coupling scheme which was widely used for interpretation of experimental Sr spectra earlier [8, 21] and, therefore, is convenient for comparing the present and previous data.

As the accuracy of calculations is less than the difference in energy for some high-lying AIS, an additional information was involved for identification of lines, i.e. their intensity behavior as a function of the incident-electron energy. The intensity $I(\alpha LSJ, J_f)$ of the line arising from the decay of the αLSJ atomic AIS [24, 25] can be written as follows:

$$I(\alpha LSJ, J_f) \sim \frac{\sigma(\alpha LSJ)}{4\pi} B(\alpha LSJ, J_f) \times \left[1 + \sum_{K>0, \text{even}}^{2J} \beta_K P_K(\cos \theta) \right]. \quad (3)$$

In (3), $B(\alpha LSJ, J_f)$ is the radiationless decay branching ratio for the αLSJ state with total orbital L , spin S and angular J momenta; J_f is the total angular momentum of a final ionic state; $\sigma(\alpha LSJ)$ is the total excitation cross section of the αLSJ state; β_K is the asymmetry coefficient of the angular

distribution of ejected electrons [26, 27]

$$\beta_K = A_K \alpha_K. \quad (4)$$

Here, A_K is the alignment parameter [25] for an excited atom in the αLSJ state, α_K is the asymmetry parameter of ejected electron due to a spontaneous decay of the αLSJ state [26]; $P_K(\cos \theta)$ is the Legendre polynomial of rank K and θ is the angle between the directions of incoming and emitted electrons (a so-called observation angle). The ejected-electron branching ratio is defined as

$$B(\alpha LSJ, J_f) = \frac{A^a(\alpha LSJ, J_f)}{\sum_i A_i^a(\alpha LSJ) + \sum_j A_j^a(\alpha LSJ, J_f)}. \quad (5)$$

Our calculations have shown that the radiative transition probabilities $A_i^r(\alpha LSJ)$ from the initial state αLSJ to all final states i are much smaller than the autoionization probabilities $A_j^a(\alpha LSJ, J_f)$, therefore

$$B(\alpha LSJ, J_f) = \frac{A^a(\alpha LSJ, J_f)}{\sum_j A_j^a(\alpha LSJ, J_f)} \quad (6)$$

can be written.

As follows from (3)–(6), the intensity of lines is proportional to the *total* excitation cross section $\sigma(\alpha LSJ)$ of corresponding AIS if the ejected-electron spectra are measured at the ‘magic’ observation angle of 54.7° and only for the states with $J = 0, 1$ ($P_2(\cos(54.7^\circ)) \simeq 0$). For other observation angles as well as for the states with $J > 1$ the asymmetry of the angular distribution of ejected electrons has to be taken into account while analyzing the excitation behaviors of lines. Its importance is well demonstrated by the difference in previous data on the number of lines and their excitation behaviors in ejected-electron spectra measured at observation angles of 75° [11, 14] and 90° [12, 13].

4. Results

4.1. Electron spectra

Examples of electron spectra at incident-electron energies E_{inc} below and above the ionization threshold of the $4p^6$ subshell at 26.92 eV [11, 21] are shown in figures 1 and 2, respectively. The analysis of the spectra in figure 1 reveals two kinds of lines between 12 and 18 eV electron energy. First, there are lines $1'–3'$, $L_1–L_2$ which shift towards higher electron energies by increment step of the energy of incident electrons (see dashed lines between the spectra). This behavior is characteristic of the energy-loss spectra in which each line corresponds to the excitation of a certain atomic level. Note, that in the spectrum at $E_{\text{inc}} = 20.90$ eV, only such type of lines is observed.

The further increase of the incident-electron energy leads to the appearance of lines at fixed energy positions. In particular, in the spectra at E_{inc} between 21.0 and 21.5 eV, the lines 42, 43, and 45 appear first. In the spectrum at $E_{\text{inc}} = 23.48$ eV, 35 lines 17–65 can already be clearly seen between 12.5 and 17.8 eV electron energy. Finally, the spectrum at $E_{\text{inc}} = 27.7$ eV (see figure 2) contains an almost

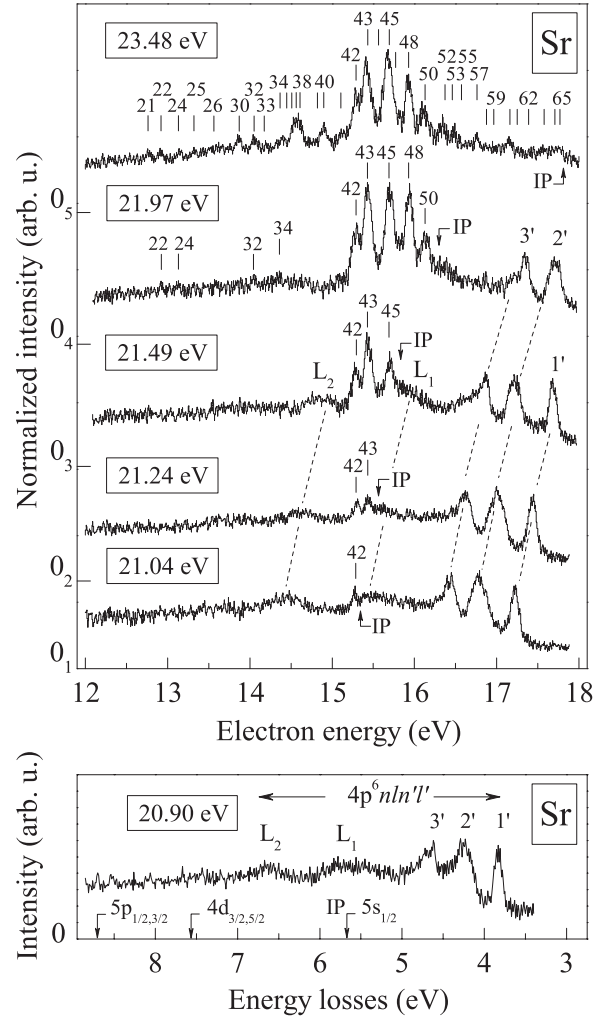


Figure 1. Electron spectra of strontium vapors for incident-electron energies $E_{\text{inc}} < 26.92$ eV (see text). Bars on top of the spectra mark the positions of ejected-electron lines. The indexation of lines is according to [11]. Labels $1'–3'$ and $L_1–L_2$ mark the energy-loss lines arising from the excitation of the $4p^6nl'n''$ levels located respectively below and above the ionization threshold $\text{IP} = 5.695$ eV [6]. The part of the spectrum at $E_{\text{inc}} = 21.49$ eV between 14 and 18 eV electron energy was used as the ‘test’ spectrum (see text).

full set of the ejected-electron lines 17–80 which correspond to the radiationless decay of the $4p^5nl'n''l'''$ atomic AIS of Sr atoms. Lines 13, 14, 16, 18–20, 23 and 27 appear in the spectra only at $E_{\text{inc}} \geq 31.7$ eV. This group corresponds to the decay of the $4p^5nl'n''$ ionic AIS with formation of Sr^{2+} in the $4p^6\ ^1S_0$ ground state. The different nature of the spectra requires their separate analysis.

Energy-loss spectra. In accordance with their positions in spectra, lines $1'–3'$ and L_1, L_2 reflect the incident-electron energy losses due to excitation of the $4p^6nl'n''$ levels located, respectively, below and above the $5s^2$ ionization threshold $\text{IP} = 5.695$ eV [6]. To our knowledge, that is the first observation of the $5s^2$ excitation process in electron energy-loss spectra. The assignment of lines $1'–3'$ was performed in accordance with the data from the NIST Atomic Spectra Database [6]. Due to the limited energy resolution of the present measurements (≈ 0.1 eV), the broad and asymmetric

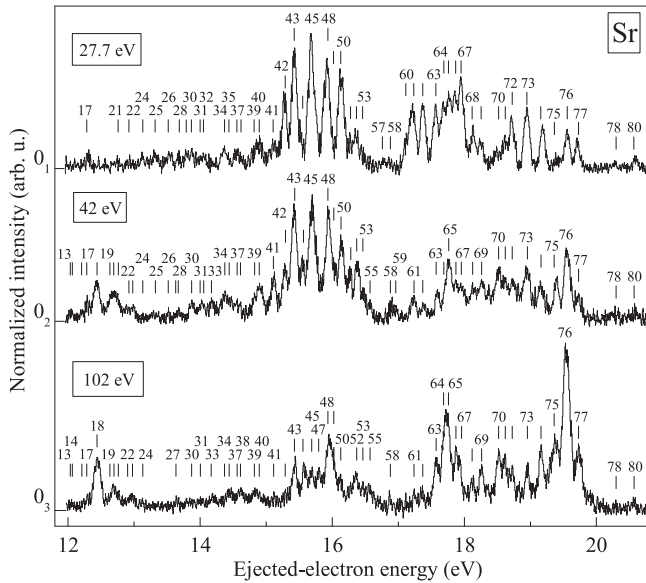


Figure 2. Ejected-electron spectra of strontium vapors for incident-electron energies $E_{\text{inc}} > 26.92$ eV. In all spectra, a polynomial background function was subtracted from the original data. The indexation of lines is according to [11].

lines 2' and 3' are, in fact, a superposition of several closely lying lines which correspond to excitation of the levels mostly from the $4d5p$, $5s6p$, $5p^2$ and $5s7s$ configurations. The maxima of both lines are formed by the dominated excitation of the $(5s6p)^1P_1$ (line 2') and $(5p^2)^1S_0 + (5s7s)^3S_1$ (line 3') levels. The line 1' is associated with excitation of the single $(5s6s)^1S_0$ level at 3.793 eV [6] and was used in calibration of the incident-electron energy scale (see section 2).

In the autoionization region between $5s_{1/2}$ and $5p_{1/2,3/2}$ ionization thresholds (see figure 1) only two broad features L_1 and L_2 at approximately 5.8 and 6.6 eV, respectively, are clearly seen in the spectrum at $E_{\text{inc}} = 20.90$ eV. The photoionization [28] and photoabsorption [29, 30] studies show that the levels $(4d^2 + 5p^2)^1D_2$, $(4d6p)^3P$, 1P_1 at 5.75 eV (46379 cm^{-1}), 6.14 eV (49547 cm^{-1}) and 6.30 eV (51099 cm^{-1}), respectively, provide main contribution to form the feature L_1 . The levels $(4d5d)^3F_2$, 1D_2 , 3P_2 , $4d6d(5/2, 5/2)_{J=0,1,2}$, $(3/2, 3/2)_{J=0}$, $(5/2, 3/2)_{J=2}$ lying between 6.3 and 6.9 eV [6] are the most likely candidates for the assignment of the feature L_2 . Finally, note that features L_1 , L_2 alter the intensity of the ejected-electron lines lying between 15.0 and 16.2 eV in the spectra at $21 \text{ eV} < E_{\text{inc}} < 22 \text{ eV}$. However, with further increasing of the incident energy, this influence becomes less noticeable (see e.g. spectrum at 23.48 eV) and, therefore, it can not change the overall excitation dynamics of ejected-electron lines.

Ejected-electron spectra. As was noted above, in the spectrum at $E_{\text{inc}} = 20.90$ eV only the energy-loss lines 1'–3' and broad features L_1 , L_2 are present. However, increasing the incident energy just by 0.14 eV leads to the appearance of the line 42 at 15.29 eV (see spectrum at $E_{\text{inc}} = 21.04$ eV in figure 1). In accordance with the analysis in section 2, this line reflects single-channel decay of the $(4p^5 4d5s^2)^3P_0$ lowest dipole-forbidden atomic AIS at 20.98 eV with a formation of Sr^+ in the $(4p^6 5s)^2S_{1/2}$ ground state. Since the first dipole-

allowed transition is seen in photoabsorption spectrum at 21.099 eV ($\lambda = 587.565 \text{ \AA}$ [8]) and there are no other states at lower excitation energies which may possess the radiative decay into $4p^6 nln'l'$ atomic states [31], the value of 20.98 ± 0.05 eV can be considered as a true excitation threshold of the $4p^6$ subshell in Sr atom. Next, in the spectra at incident-electron energies of 21.24 and 21.49 eV, the lines 43 and 45 appear. A further increase of the electron beam energy up to 21.97 eV leads to the appearance of two groups of lines 22, 32, 48 and 24, 34, 50 with excitation thresholds at approximately 21.6 and 21.8 eV, respectively. The simultaneous appearance and similar excitation dynamics of lines in each group indicate their common origin, namely, the multichannel radiationless decay of the atomic AIS.

In the previous studies of ejected-electron spectra of alkali atoms (see [16, 19] and references therein) it was found that due to different excitation dynamics of dipole-allowed (total momentum $J = 1$) and dipole-forbidden ($J \neq 1$) atomic states the structure of the spectra measured at low and high impact energies are noticeably different both in intensity and in number of lines. In particular, the high-energy spectra contain significantly fewer lines which can be associated, in accordance with their excitation dynamics, with dipole-allowed states. This behavior, being true even for the spectra of heaviest Cs atoms [16, 32], facilitated to a considerable degree the accurate identification of lines in ejected-electron spectra of alkali atoms. However, the different situation was recently observed in electron spectra of Ba atoms [17] where only five lines show the clear dipole-forbidden excitation character of corresponding AIS. It is of interest, therefore, to analyze the spectra of Sr atoms in the same way.

Even a cursory analysis of the spectra in figures 1, 2 shows that their structure becomes more complex with increasing the incident-electron energy. A closer analysis shows that almost all lines seen in the spectra at low incident-electron energies (see spectra at 23.48 and 27.7 eV) are clearly observed also in the spectrum at 102 eV, as well as in the spectra measured earlier at 200 [13] and 500 eV [11] incident energies. Moreover, many of these lines retain sufficiently high intensity (see, e.g., lines 43–55). In fact, there are only four lines 28, 29, 57 and 59 which excitation behaviors point out the dipole-forbidden excitation character of corresponding states. Thus, this situation is completely analogous to that of barium and is a result of strong mixing processes accompanying p^6 excitation in these atoms (see section 4.2). However, as the results of the identification of lines show (see Discussion below), the effect of superposition of lines from different decay channels can be an additional factor which may also alter their excitation dynamics.

In the ejected-electron energy range 12–21 eV which was studied in the present work, 52 lines with excitation thresholds below 26.92 eV ionization energy of the $4p^6$ subshell were revealed in the spectra. No new lines were observed if comparing with previous data [10–14]. Since the excitation threshold of the $4p^6$ subshell was established at 20.98 eV, a group of lines 17, 21, 22, 24–41 with ejected-electron energies less than 15.29 eV (line 42) can not be associated with autoionizing transitions to the $5s_{1/2}$ Sr^+ state but with the

Table 1. Calculated excitation energies (E , eV), cross sections (σ , Mb) at 23.5, 27.7, 42 and 102 eV incident-electron energy, decay branching ratios (B) (6) to $4p^6nlj$ states of Sr^+ for the $4p^5nl(L_1S_1)n'l'(L_2S_2)n''l''LSJ$ AIS of Sr atoms used for the identification of lines observed in ejected-electron spectra. The numbering is given according to the full list of 29824 states included in the calculations. The value of B in brackets represents a branching ratio with included $4p^5nl n'l'$ decay channels.

State	Configuration LSJ	E	σ				B			
			23.5	27.7	42	102	$5s_{1/2}$	$4d_{3/2}^{3/2}$	$5p_{3/2}^{1/2}$	$6s_{1/2}$
103	$4d5s^2\ ^3P_0$	20.961	10.65	6.72	3.12	1.34	0.82	$\frac{0.07}{0.02}$	$\frac{0.03}{0.06}$	
104	$4d5s^2\ ^3P_1$	21.134	31.29	19.38	9.16	5.27	0.81	$\frac{0.07}{0.03}$	$\frac{0.06}{0.05}$	
105	$4d5s^2\ ^3P_2$	21.432	48.84	29.11	13.81	0.59	0.78	$\frac{0.03}{0.03}$	$\frac{0.07}{0.02}$	
106	$4d5s^2\ ^3F_4$	21.685	35.11	20.14	9.53	0.39	0.71	$\frac{0.09}{0.00}$	$\frac{0.08}{0.00}$	
107	$4d5s^2\ ^3F_3$	21.841	24.90	14.51	6.73	0.71	0.63	$\frac{0.15}{0.18}$	$\frac{0.13}{0.03}$	
110	$4d5s^2\ ^3F_2$	22.121	16.49	9.06	2.55	0.14	0.40	$\frac{0.04}{0.38}$	$\frac{0.12}{0.03}$	
112	$5s^25p\ ^3P_1$	22.243	4.40	2.32	0.73	0.05	0.52	$\frac{0.06}{0.08}$	$\frac{0.12}{0.07}$	
117	$4d^2(^3P)(^4P)5s\ ^5P_3$	22.364	0.53	0.29	0.14	0.03	0.03	$\frac{0.05}{0.01}$	$\frac{0.27}{0.04}$	
121	$4d5s^2\ ^3D_3$	22.504	11.27	6.59	3.44	1.13	0.03	$\frac{0.84}{0.02}$	$\frac{0.07}{0.02}$	
123	$5s^25p\ ^3D_3$	22.601	3.50	1.86	0.72	0.04	0.27	$\frac{0.83}{0.00}$	$\frac{0.09}{0.11}$	
124	$5s^25p\ ^3D_2$	22.611	1.76	1.03	0.54	0.18	0.15	$\frac{0.31}{0.07}$	$\frac{0.31}{0.38}$	
125	$5s^25p\ ^1P_1$	22.644	0.98	0.50	0.05	0.01	0.04	$\frac{0.03}{0.05}$	$\frac{0.36}{0.60}$	
128	$5s^25p\ ^3P_2$	22.732	1.27	0.91	0.70	0.37	0.18	$\frac{0.00}{0.03}$	$\frac{0.30}{0.01}$	
129	$4d5s^2\ ^3D_1$	22.731	5.75	3.64	2.19	1.13	0.06	$\frac{0.01}{0.73}$	$\frac{0.76}{0.07}$	
132	$4d5s^2\ ^1D_2$	22.858	8.98	4.67	1.93	0.07	0.07	$\frac{0.10}{0.27}$	$\frac{0.03}{0.09}$	
133	$4d(^3P)5s(^4P)5p\ ^3P_1$	22.876	0.94	0.47	0.17	0.01	0.05	$\frac{0.54}{0.00}$	$\frac{0.02}{0.20}$	
138	$5s^25p\ ^3D_1$	23.057	0.57	0.29	0.18	0.01	0.13	$\frac{0.02}{0.05}$	$\frac{0.72}{0.77}$	
142	$4d5s^2\ ^3D_2$	23.129	13.22	6.71	1.85	0.015	0.44	$\frac{0.00}{0.30}$	$\frac{0.02}{0.08}$	
143	$5s^25p\ ^1D_2$	23.162	0.72	0.53	0.37	0.27	0.18	$\frac{0.17}{0.01}$	$\frac{0.00}{0.02}$	
144	$4d5s^2\ ^1F_3$	23.178	5.41	4.11	3.20	1.94	0.33	$\frac{0.06}{0.53}$	$\frac{0.06}{0.05}$	
145	$4d^2(^3P)(^4P)5s\ ^5P_2$	23.182	1.48	0.78	0.41	0.01	0.52	$\frac{0.17}{0.23}$	$\frac{0.02}{0.05}$	
154	$4d^2(^3P)(^5P)5s\ ^5P_1$	23.362	0.25	0.16	0.10	0.06	0.14	$\frac{0.59}{0.19}$	$\frac{0.00}{0.06}$	
157	$4d^2(^3F)(^2F)5s\ ^3F_2$	23.397	2.14	1.15	0.48	0.02	0.70	$\frac{0.24}{0.02}$	$\frac{0.02}{0.01}$	0.01
159	$4d^2(^3F)(^4D)5s\ ^3D_1$	23.434	2.98	1.79	1.32	0.63	0.14	$\frac{0.63}{0.18}$	$\frac{0.02}{0.01}$	
161	$4d^2(^3F)(^4G)5s\ ^5G_2$	23.508		1.53	0.68	0.02	0.57	$\frac{0.27}{0.12}$	$\frac{0.03}{0.01}$	0.03
162	$4d^2(^1D)(^2D)5s\ ^3D_3$	23.533		2.17	1.25	0.48	0.67	$\frac{0.19}{0.17}$	$\frac{0.01}{0.45}$	0.01
165	$4d^2(^3P)(^4P)5s\ ^5D_0$	23.611		0.65	0.73	0.34	0.50	$\frac{0.03}{0.01}$	$\frac{0.01}{0.35}$	
168	$4d^2(^3F)(^4F)5s\ ^5F_5$	23.661		0.76	0.73	0.39	0.48	$\frac{0.12}{0.05}$	$\frac{0.01}{0.01}$	
173	$4d^2(^3F)(^4F)5s\ ^5F_1$	23.762		1.92	1.54	0.78	0.74	$\frac{0.22}{0.02}$	$\frac{0.00}{0.01}$	
176	$4d^2(^3F)(^4F)5s\ ^5F_2$	23.818		1.30	0.24	0.01	0.84	$\frac{0.09}{0.01}$	$\frac{0.01}{0.01}$	0.02
179	$4d^2(^3F)(^4F)5s\ ^5F_3$	23.856		1.22	0.53	0.11	0.14	$\frac{0.59}{0.24}$	$\frac{0.00}{0.01}$	
185	$4d^2(^1D)(^2P)5s\ ^3P_1$	23.934		0.21	0.14	0.08	0.44	$\frac{0.30}{0.19}$	$\frac{0.03}{0.03}$	
187	$4d^2(^1D)(^2P)5s\ ^3P_2$	23.980		0.57	0.25		0.71	$\frac{0.05}{0.19}$	$\frac{0.02}{0.01}$	0.01
188	$4d^2(^3P)(^4P)5s\ ^3P_2$	23.988		1.68	0.53	0.05	0.05	$\frac{0.22}{0.66}$	$\frac{0.03}{0.03}$	0.01

State	Configuration LSJ	E	σ			B				
			27.7	42	102	$5s_{1/2}$	$4d_{3/2}^{3/2}$	$5p_{3/2}^{1/2}$	$6s_{1/2}$	$5d_{3/2}^{3/2}$
191	$4d(^3P)5s(^2P)5p\ ^3D_2$	24.048	1.71	1.76	0.91	0.44	$\frac{0.07}{0.07}$	$\frac{0.16}{0.24}$		
193	$4d^2(^3P)(^4D)5s\ ^3D_3$	24.053	2.31	0.95	0.15	0.83	$\frac{0.00}{0.12}$		0.02	
199	$4d^2(^3P)(^4P)5s\ ^3P_1$	24.141	1.13	0.80	0.45	0.44	$\frac{0.40}{0.10}$	$\frac{0.01}{0.01}$	0.01	
204	$4d^2(^1D)(^2D)5s\ ^1D_2$	24.219	1.20	0.43	0.01	0.57	$\frac{0.36}{0.03}$	$\frac{0.01}{0.02}$		

Table 1. (Continued.)

State	Configuration <i>LSJ</i>	<i>E</i>	σ			<i>B</i>				
			27.7	42	102	5s _{1/2}	4d _{3/2} ^{5/2}	5p _{3/2} ^{1/2}	6s _{1/2}	5d _{3/2} ^{5/2}
207	5s ² 5p ³ D ₁	24.260	0.45	0.13	0.01	0.59	0.10 0.04 0.29	0.14 0.13 0.01		
210	4d ² (¹ D)(² D)5s ³ D ₁	24.291	0.82	0.70	0.37	0.35	0.30 0.11	0.04 0.28		0.00 0.01
213	5s ² 5p ³ P ₁	24.349	0.57	0.07		0.05	0.12 0.50	0.41 0.01		
233	4d ² (³ F)(⁴ F)5s ³ F ₂	24.564	0.78	0.20	0.01	0.37	0.09 0.21	0.02 0.01	0.01	
258	5s ² 6s ³ P ₂	24.866	0.59	0.23	0.08	0.21	0.43	0.02	0.08	0.01 0.02
264	4d(³ F)5s(² F)5p ¹ D ₂	24.909	5.08	5.23	2.91	0.95				
277	4d(³ P)5s(⁴ P)6s ³ P ₂	25.013	0.76	0.32	0.01	0.35	0.07 0.11 0.08	0.00 0.03 0.01	0.40	0.02 0.02 0.02
281	5s ² 6s ¹ P ₁	25.038	0.56	0.61	0.58	0.23	0.07 0.07	0.01 0.01	0.56	0.02 0.02
288	4d(³ P)5s(² P)6s ¹ P ₁	25.083	0.54	0.68	0.64	0.32	0.08 0.07	0.01 0.06	0.47	0.02 0.04
339	5s(³ P)5p(¹ D) ³ P ₁	25.382	2.07	1.68	1.08	0.40	0.11 0.14	0.25 0.06	0.04	0.03 0.04
373	4d(³ P)5s(⁴ P)5d ³ P ₁	25.535	2.10	2.10	1.53	0.54	0.01 0.10	0.06 0.06	0.12	0.02 0.05
377	4d(¹ D)5s(² D)6s ³ D ₁	25.551	4.34	4.51	3.50	0.59	0.11 0.09	0.04 0.02		0.03 0.01
379	4d(³ F)5s(⁴ F)7s ⁵ F ₁	25.560	0.70	0.75	0.50	0.57	0.17 0.07	0.01 0.02	0.12	0.01 0.03
389	4d(³ P)5s(⁴ P)7s ³ P ₁	25.599	2.10	2.36	1.81	0.68	0.07 0.09	0.05 0.00	0.07	0.02 0.03
474	4d(³ F)5s(² F)5d ¹ P ₁	25.906	0.26	0.38	0.35	0.12	0.24 0.08	0.03 0.03	0.44	0.04 0.50
478	4d(³ P)5s(² P)5d ³ D ₁	25.916	0.44	0.46	0.34	0.27	0.04 0.03	0.01 0.45		0.06 0.17
606	5s ² 6d ³ P ₁	26.213	0.76	0.81	0.61	0.18	0.10 0.01	0.01 0.19	0.01	0.04 0.14
614	4d(³ P)5s(² P)6d ³ P ₁	26.228	0.48	0.35	0.24	0.17	0.15 0.11	0.19 0.25	0.12	0.02 0.09
760	4d(³ P)5s(² P)6d ³ D ₁	26.528	0.49	0.46	0.28	0.31	0.01 0.11	0.10 0.02	0.04	0.08 0.08
1165	4d(³ F)5s(⁴ F)7d ³ D ₁	27.043	2.17	2.14	1.56	0.40	0.08 0.04	0.27 0.01	0.05	0.00 0.05
1184	4d(³ F)5s(⁴ F)7d ⁵ F ₁	27.060	2.03	2.28	1.63	0.35	0.14 0.06	0.27 0.08	0.02	0.12 0.05
1404	4d(³ F)5s(⁴ F)7d ⁵ P ₁	27.341	2.27	8.47	2.10	0.52	0.20 0.15	0.03 0.03		0.07 0.22
1493	4d(¹ D)5s(² D)7d ⁵ P ₁	27.443	0.47	0.43	0.32	0.20	0.03	0.09	0.12	0.16
2277	4d ² (³ P)(² P)7s ³ P ₁	28.140		1.09	0.79	(0.07)	(0.01) (0.01)	(0.01) (0.03)		(0.00) (0.02)
3172	4d(³ P)5p(⁴ P)6p ⁵ P ₁	28.761		0.15	0.12	(0.01)				(0.02) (0.00)
3327	4d ² (³ F)(⁴ F)7d ⁵ F ₁	28.852		1.32	0.93	(0.09)	(0.07) (0.00)	(0.00) (0.16)		

autoionizing transitions into the 4d_{3/2,5/2} or higher Sr⁺ excited states.

The identification of the lines observed in the ejected-electron spectra of Sr atoms is carried out as follows. First, by the comparative analysis of the experimental ejected-electron energies *E*_{ejc} and the energy structure of the 4p⁶*nl* ionic levels [6] the excitation energies *E*_{exc} of the 4p⁵*nl**n'**l'**n''l''* states which may possess the autoionizing transitions into the 4p⁶5s, 4d, 5p, 6s and 5d states of Sr⁺ are determined. Second, in order to distinguish dipole-allowed AIS which serve as milestones in the alignment of the whole energy level scheme, the obtained data are compared with the calculated energies of the states with *J* = 1 in odd configurations as well as with the energies of lines observed in photoabsorption spectra [7–9]. The final decision on the identification of a particular line is made if there is a correlation between its excitation behavior observed in experimental spectra and the calculated values of the excitation cross section and Auger yield for a particular AIS.

4.2. Calculations

Calculated excitation energies (*E*, eV), cross sections (σ , Mb) at 23.5, 27.7, 42 and 102 eV incident-electron energy, decay

branching ratios (*B*) (6) to 4p⁶*nlj* states of Sr⁺ for the 4p⁵*nl*(*L*₁*S*₁)*n'**l'*(*L*₂*S*₂)*n''l''LSJ* AIS of Sr atoms used for the identification of lines observed in ejected-electron spectra are presented in table 1. The numbering is given according to the full list of 29824 states included in the calculations.

The assignment of the states was performed using the largest expansion coefficient. If the first expansion coefficient of a particular state was used for other levels, the second or third one was chosen such to avoid the assignment of the same term for two levels. The first largest expansion coefficient was obtained only for a part of the low-lying levels of the configurations 4p⁵4d5s², 4p⁵4d²5s² and 4p⁵4d²5g both in *LSJ* and *jjJ* coupling schemes. For all other levels, the mixing effects are stronger resulting in expansion coefficients less than 0.5. Note that the absence of a dominant term leads to the disappearance of some levels from the spectrum. Such effect was earlier observed in barium [17] for the ¹P₁ level from the 5p⁵5d6s² configuration. The present calculations show that the highest level ¹P₁ of the 4p⁵4d5s² configuration is also absent in Sr spectrum, as the radial orbital 4d is localized in the outer well of a potential [33] if term-dependent calculations are performed. In average single configuration

approximation, 4d radial orbital for 1P_1 state is localized in the inner well, and its energy obtained is too large comparing to term-dependent calculation. The use of the superposition of $4p^5nd$ ($n = 4, 5, 6, \dots$) configurations [33] is equivalent to the term-dependent calculation and shifts down the 1P_1 state to right place, but the dominant expansion coefficient is lost. This state is represented by many expansion coefficients which values are smaller than 0.2. The expansion coefficients less than 0.4 were obtained also for the 3D_1 , 1D_2 and 3P_2 levels in the $4p^54d5s^2$ configuration and for some levels in more higher excited configurations.

The present calculated excitation energies of the states with $J = 1$ of odd configurations were compared to those calculated in configuration-interaction approximation using the basis of numerical solutions of Hartree–Fock equations in the quasi-relativistic approximation and by scaling down *ab initio* Slater–Condon parameters [8]. This comparison shows that the latter results are shifted down by around 0.04–0.09 eV, for all considered states. The similar comparison of the assignment of quantum numbers LS is complicated as the superposition of much more configurations was used in the present work. Thus, the expansion coefficients are distributed among more configurations. In [8], the greatest LS -component was used for the assignment of quantum numbers but the same LS -assignment was sometimes used for more than one level as many percentages were much less than 50%. In the present work, only one assignment was used for one level, therefore, the intermediate and the final quantum numbers LS differ of many cases from those presented in [8].

Parameters B were calculated for the autoionizing transitions to the singly excited $4p^6nLS$ ($nl = 5s, 4d, 5p, 6s, 5d$) Sr^+ states. Beginning with state 1139, transitions to the core-excited $4p^55s^2LS$, $4p^54d^2LS$ and $4p^54d5d$ LS states become energetically allowed and they were taken into account. The contribution of these transitions in the denominator of (6) increases with the excitation energy of the decaying state. For example, the parameter B decreases by 10.75, 27, and 1.8 times for the states 2277, 3172 and 3327, respectively (see data in brackets), comparing with the case when transitions to core-excited states of Sr^+ are not taken into account.

5. Discussion

The analysis of the experimental and calculated data has resulted in the identification of the 60 ejected-electron lines observed both in the present study and in earlier experiments [10, 11, 13]. Also, the present calculations are used to reconsider the identification of the 68 most intense lines in the photoabsorption spectra [7–9]. The parameters of 105 classified states $4p^5nl'n''l'''$ which define the $4p^6$ energy spectrum of Sr atoms between 20 and 29 eV are shown in table 2. Below in section 5.1 we discuss regularities and peculiarities of excitation (1) and decay (2) processes for these states. In section 5.2, the identification of photoabsorption lines is considered.

5.1. Ejected-electron spectra

Single-excited configurations. The configuration $4p^54d5s^2$ is the lowest and the most efficiently excited in the $4p^6$ energy spectrum of Sr atoms. Due to strong mixing effects (see analysis in section 4.2) of 12 states of this configuration the decay of only 11 states 103–110, 121, 129, 132, 142, 144 is observed in the ejected-electron spectra. The large Auger yields for the transitions into $Sr^+ 5s_{1/2}$ ground state (see table 1) predict the single-channel decay mode for the lowest AIS 3P_0 (103), 3P_1 (104) and 3P_2 (105). The excitation behavior of lines 42, 43 and 45 perfectly confirms this. For the remaining eight states, the most likely are two or three decay channels with Sr^+ ions formed in the $5s_{1/2}$, $4d_{3/2,5/2}$ and $5p_{1/2,3/2}$ states. Note that the lines 42, 43, 45, 48, 50, and 52 form the most intensive part of the ejected-electron spectra at low and medium impact energies (see figures 1, 2). The 3P_1 (104) and 3D_1 (129) states are the lowest dipole-allowed core-excited AIS which give rise to the $4p^6$ -subshell photoabsorption spectrum of Sr atoms [8].

In accordance with the data in table 1, the next in excitation energy and excitation efficiency is the even configuration $4p^55s^25p$. The lines 26, 28–30, 53, 57, 58, 60 and 70 with moderate intensities are associated with a multichannel decay of nine states occupying a narrow energy region of 2 eV above the excitation threshold of the $4p^6$ subshell. Note that even in this low-energy spectral region adding only one configuration greatly complicates the unambiguous identification of lines due to both the closeness of excitation energies of the states and their multichannel decay mode. For example, for two groups of states 121, 123, 124 and 142–144 ($\Delta E < 0.02$ eV) the identification became possible only in the presence of the calculated cross sections and decay rates and introducing the concept of satellite lines, i.e., virtual lines which coincide in energy with the lines observed in ejected-electron spectra but correspond to the different decay channels. As can be seen from table 2, almost all ejected-electron lines observed in spectra have satellite lines of the same energy. However, by comparing the cross sections and decay rates of close-lying AIS, it is possible to evaluate the contribution from different decay channels (or, in other words, the role of satellite lines) to the intensity of a particular spectral line. For example, such analysis performed for the states 123 and 124 showed that the intensity of the line 57 is determined mainly by the $5s_{1/2}$ decay channel of the state $5s^25p^3D_3$ (123) while the $5p_{3/2}$ decay channels of both states contribute approximately equally to the intensity of the line 28. A similar conclusion can be made also about the role of decay channels $5p_{1/2}$ and $5p_{3/2}$ of the states $5s^25p^3D_1$ (138) and $5s^25p^1D_2$ (143), respectively, in formation of the intensity of the line 33.

For high-energy states, the calculations and photoabsorption data become the only tools for conducting a more or less reliable classification. Thus, 13 states 258, 281, 523, 542, 606, 614, 1602, 1650, 1658, 2285, 3178, 3364 and 3389 are classified as dipole-allowed states belonging to the high-lying $4p^55s^2nl$ configurations ($nl = 6s, 7s, 6d, 7d, 8d, 9s$). Only line 78 and five satellites 25', 28'', 59', 62'' and 78' are

Table 2. The energy structure and decay channels of the $4p^5nh'l'n''l''LSJ$ states in Sr atoms.

State	E_{exc}			Configuration LSJ	Decay channel	E_{ejc} , eV	Line
	Theory, eV	Experiment					
		Present, eV	[8], Å (eV)				
103	20.961	20.98		$4d\ 5s^2\ ^3P_0$	$5s_{1/2}$	15.29	42
104	21.134	21.12	587.565 (21.099)	$4d\ 5s^2\ ^3P_1$	$5s_{1/2}$	15.43	43
105	21.432	21.38		$4d\ 5s^2\ ^3P_2$	$5s_{1/2}$	15.69	45
106	21.685	21.62		$4d\ 5s^2\ ^3F_4$	$5s_{1/2}$	15.93	48
					$4d_{5/2}$	14.05	32
					$5p_{3/2}$	12.92	22
					$5s_{1/2}$	16.13	50
107	21.841	21.82		$4d\ 5s^2\ ^3F_3$	$4d_{3/2}$	14.37	34
					$5p_{3/2}$	13.13	24
					$5s_{1/2}$	16.37	52
110	22.121	22.06		$4d\ 5s^2\ ^3F_2$	$4d_{3/2}$	14.56	37
					$5p_{3/2}$	13.33	25
					$5s_{1/2}$	16.53	53
112	22.243	22.22		$5s^25p\ ^3P_1$	$5p_{3/2}$	13.52	26
					$4d_{5/2}$	14.82	39
117	22.364	22.35		$4d^2(^3P)(^4P)5s^5P_3$	$4d_{5/2}$	14.90	40
121	22.504	22.43		$4d\ 5s^2\ ^3D_3$	$5s_{1/2}$	16.76	57
123	22.601	22.45		$5s^25p\ ^3D_3$	$4d_{5/2}$	14.92	40 ^{''a}
					$5p_{1/2}$	13.80	29
					$5p_{3/2}$	13.67	28
					$5s_{1/2}$	16.76	57'
124	22.611	22.46		$5s^25p\ ^3D_2$	$5p_{1/2}$	13.80	29'
					$5p_{3/2}$	13.67	28'
					$5s_{1/2}$	16.88	58
125	22.644	22.51		$5s^25p\ ^1P_1$	$5p_{1/2}$	13.87	30
					$5p_{3/2}$	13.80	29 ^{''a}
128	22.732	22.57		$5s^25p\ ^3P_2$	$5p_{3/2}$	13.87	30'
					$5s_{1/2}$	16.88	58'
129	22.736	22.61	548.75 (22.592)	$4d\ 5s^2\ ^3D_1$	$5s_{1/2}$	16.88	58'
					$4d_{3/2}$	15.11	41
132	22.858	22.66		$4d\ 5s^2\ ^1D_2$	$5s_{1/2}$	16.96	59
					$4d_{3/2,5/2}$	15.11	41'
133	22.876	22.73		$4d(^3P)5s(^4P)5p^3P_1$	$5p_{1/2}$	14.05	32'
					$5p_{3/2}$	14.00	31
138	23.057	22.80		$5s^25p\ ^3D_1$	$5s_{1/2}$	17.15	60
					$5p_{1/2}$	14.17	33
142	23.129	22.93		$4d\ 5s^2\ ^3D_2$	$5s_{1/2}$	17.24	61
					$4d_{3/2}$	15.43	43'
143	23.162	22.94		$5s^25p\ ^1D_2$	$5p_{3/2}$	14.17	33'
144	23.178	22.94		$4d\ 5s^2\ ^1F_3$	$5s_{1/2}$	17.24	61'
					$4d_{5/2}$	15.43	43''
145	23.182	22.94		$4d^2(^3P)(^4P)5s\ ^5P_2$	$5s_{1/2}$	17.24	61''
154	23.362	23.07	537.346 (23.072)	$4d^2(^3P)(^4P)5s\ ^5P_1$	$5s_{1/2}$	17.37	62
					$4d_{3/2,5/2}$	15.57	44
157	23.397	23.07		$4d^2(^3F)(^2F)5s\ ^3F_2$	$5s_{1/2}$	17.37	62'
159	23.434	23.11	535.893 (23.134)	$4d^2(^3F)(^4D)5s\ ^3D_1$	$4d_{3/2,5/2}$	15.57	44'
161	23.508	23.26		$4d^2(^3F)(^4G)5s^5G_2$	$5s_{1/2}$	17.57	63
					$4d_{3/2,5/2}$	15.75	46
162	23.533	23.27		$4d^2(^1D)(^2D)5s\ ^3D_3$	$5s_{1/2}$	17.57	63'

Table 2. (Continued.)

State	E_{exc}		Configuration LSJ	Decay channel	E_{ejc} , eV	Line	
	Theory, eV	Experiment					
		Present, eV					[8], Å (eV)
				4d _{3/2}	15.75	46'	
165	23.611	23.38	4d ² (³ P)(⁴ P)5s ⁵ D ₀	5s _{1/2}	17.69	64	
168	23.661	23.38	4d ² (³ F)(⁴ F)5s ⁵ F ₅	5s _{1/2}	17.69	64'	
173	23.762	23.39	530.064 (23.389)	4d ² (³ F)(⁴ F)5s ⁵ F ₁	5s _{1/2}	17.76	64''
				4d _{3/2}	15.93	48'	
176	23.818	23.45	4d ² (³ F)(⁴ F)5s ⁵ F ₂	5s _{1/2}	17.76	65	
179	23.856	23.52	4d ² (³ F)(⁴ F)5s ⁵ F ₃	4d _{3/2}	16.02	49	
185	23.934	23.57	525.359 (23.598)	4d ² (¹ D)(² P)5s ³ P ₁	5s _{1/2}	17.87	66
				4d _{3/2,5/2}	16.02	49'	
187	23.980	23.64	4d ² (¹ D)(² P)5s ³ P ₂	5s _{1/2}	17.95	67	
188	23.988	23.66	4d ² (³ P)(⁴ P)5s ³ P ₂	4d _{3/2,5/2}	16.28	50'	
191	24.048	23.66	4d(³ P)5s(² P)5p ³ D ₂	5s _{1/2}	18.72	67'	
193	24.053	23.67	4d ² (³ P)(⁴ D)5s ³ D ₃	5s _{1/2}	18.72	67''	
199	24.141	23.82	521.293 (23.782)	4d ² (³ P)(⁴ P)5s ³ P ₁	5s _{1/2}	18.12	68
				4d _{3/2}	16.31	51	
204	24.219	23.95	4d ² (¹ D)(² D)5s ¹ D ₂	5s _{1/2}	18.26	69	
				4d _{3/2}	16.45	53'	
207	24.263	24.22	5s ² 5p ³ D ₁	5s _{1/2}	18.52	70	
210	24.291	24.32	510.731 (24.274)	4d ² (¹ D)(² D)5s ³ D ₁	5s _{1/2}	18.62	71
				4d _{5/2}	16.76	57''	
213	24.349	24.33	5s ² 5p ³ P ₁	5p _{1/2}	15.69	45'	
				5p _{3/2}	15.57	44''	
233	24.564	24.42	4d ² (³ F)(⁴ F)5s ³ F ₂	5s _{1/2}	18.72	72	
				4d _{3/2}	16.88	58''	
258	24.866	24.49	5s ² 6s ³ P ₂	4d _{5/2}	16.96	59'	
264	24.909	24.65	4d(³ F)5s(² F)5p ¹ D ₂	5s _{1/2}	18.95	73	
277	25.013	24.85	4d(³ P)5s(⁴ P)6s ³ P ₂	5s _{1/2}	19.16	74	
281	25.038	24.93	496.885 (24.950)	5s ² 6s ¹ P ₁	6s _{1/2}	13.32	25'
288	25.083	25.05	494.91 (25.050)	4d(³ P)5s(² P)6s ¹ P ₁	5s _{1/2}	19.36	75
339	25.382	25.11	493.910 (25.101)	5s(³ P)5p ² (¹ D) ³ P ₁	5s _{3/2}	19.42	24 ^b
				5p _{3/2}	16.37	52'	
373	25.535	25.21	491.84 (25.206)	4d(³ P)5s(⁴ P)5d ³ P ₁	5s _{1/2}	19.52	76a
377	25.551	25.25	490.92 (25.254)	4d(¹ D)5s(² D)6s ³ D ₁	5s _{1/2}	19.56	76b
379	25.560	25.28	489.750 (25.314)	4d(³ F)5s(⁴ F)7s ⁵ F ₁	5s _{1/2}	19.59	76c(27 ^b)
389	25.599	25.42	488.028 (25.403)	4d(³ P)5s(⁴ P)7s ³ P ₁	5s _{1/2}	19.73	77
428	25.752	487.557 (25.428)	4d(³ P)5s(⁴ P)6d ⁵ F ₁				
432	25.776	485.943 (25.512)	4d(¹ D)5s(² D)5d ³ P ₁				
447	25.829	484.969 (25.563)	4d ² (³ P)(² S)5s ³ S ₁				
474	25.906	25.61	484.210 (25.604)	6s7s ² ¹ P ₁	6s _{1/2}	14.00	31'
478	25.916	25.62	483.351 (25.649)	4d(³ P)5s(² P)5d ³ D ₁	5d _{3/2}	13.32	25''
507	26.001	482.789 (25.679)	5s8s ² ¹ P ₁				
523	26.034	481.185 (25.765)	5s ² 6d ¹ P ₁				
542	26.069	479.145 (25.845)	5s ² 7s ¹ P ₁				
562	26.118	479.145 (25.874)	6s ² 7s ¹ P ₁				
579	26.165	478.522 (25.908)	4d(³ F)5s(⁴ F)5d ³ P ₁				
606	26.213	25.99	477.09 (25.986)	5s ² 6d ³ P ₁	5s _{1/2}	20.30	78
				5p _{1/2}	17.37	62''	
				5d _{3/2}	13.69	28''	
614	26.228	25.99	476.602 (26.012)	5s ² 6d ³ P ₁	5s _{1/2}	20.30	78'
631	26.275	476.077 (26.041)	4d(³ P)5s(⁴ P)7d ⁵ D ₁				

Table 2. (Continued.)

State	E_{exc}		Configuration LSJ	Decay channel	E_{ejc} , eV	Line	
	Theory, eV	Experiment					
		Present, eV					[8], Å (eV)
656	26.357		475.822 (26.055)	4d(³ D)5p(² P) ³ D ₁			
678	26.413		475.343 (26.081)	4d(³ F)5s(⁴ F)6d ³ P ₁			
760	26.528	26.15	473.752 (26.169)	4d(³ P)5s(² P)6d ³ D ₁	5s _{1/2}	20.46 79	
1165	27.043	26.26	471.987 (26.267)	4d(³ F)5s(⁴ F)7d ⁵ D ₁	5s _{1/2}	20.57 80	
1173	27.046		470.405 (26.355)	4d(³ F)5s(⁴ F)5g ⁵ F ₁			
1184	27.060	26.49	468.227 (26.478)	4d(³ F)5s(⁴ F)7d ⁵ F ₁	5s _{1/2} 5p _{3/2}	20.80 81 17.76 65'	
1198	27.081		467.442(26.522)	4d(² G)(² F)6d ³ P ₁			
1258	27.115		467.327 (26.529)	4d(³ F)5s(² F)6d ¹ P ₁			
1278	27.180		467.086 (26.542)	4d(² F)(² D)7d ³ P ₁			
1389	27.312		466.174 (26.594)	4d(³ D)5s(⁴ D)6d ³ S ₁			
1404	27.341	26.67	464.991 (26.662)	4d(³ P)5s(² P)7d ¹ P ₁	5s _{1/2} 4d _{5/2}	20.98 82 19.16 74'	
1416	27.356		464.545 (26.687)	4d(³ F)5s(⁴ F)7d ⁵ F ₁			
1450	27.398		463.132 (26.769)	4d(³ F)5s(² F)7d ¹ P ₁			
1474	27.417		462.768 (26.790)	4d(² D)(² P)7s ³ P ₁			
1482	27.427		462.593 (26.800)	4d(³ F)5s(⁴ F)7d ⁵ D ₁			
1493	27.443	26.88	461.090 (26.887)	4d(³ D)5s(⁴ D)7d ⁵ P ₁	5s _{1/2} 5d _{3/2}	21.19 83 14.61 38	
1512	27.610		460.521 (26.921)	4d(¹ D)5s(² D)7d ³ D ₁			
1602	27.567		459.762 (26.965)	5s ² 8d ³ P ₁			
1650	27.610		459.464 (26.983)	5s ² 9s ¹ P ₁			
1658	27.615		458.475 (27.041)	5s ² 8d ¹ P ₁			
1703	27.655		457.683 (27.088)	4d(² F)(² D)7s ³ D ₁			
1719	27.669		456.901 (27.134)	5d6s ² ³ D ₁			
1814	27.739		455.638 (27.209)	6s ² 6d ³ P ₁			
1851	27.774		455.530 (27.216)	4d6s ² ³ D ₁			
2129	27.984		451.489 (27.459)	4d(³ P)5s(⁴ P)7d ⁵ D ₁			
2229	28.089		449.906 (27.556)	4d(³ D)5s(⁴ D)7d ³ P ₁			
2277	28.140	27.77	446.425 (27.771)	4d(² P)(⁴ P)7s ⁵ P ₁	5s _{1/2}	22.08 69 ^c	
2285	28.149		445.230 (27.845)	5s ² 7d ³ D ₁			
2415	28.246		444.962 (27.862)	4d(³ F)5s(² F)8d ¹ P ₁			
2558	28.368		444.776 (27.874)	4d(³ F)5p(² P) ⁵ F ₁			
3145	28.748		438.82 (28.252)	4d(² G)(² H)5g ¹ P ₁			
3156	28.752		438.70 (28.260)	5s(³ P)5p(⁴ S)6p ⁵ P ₁			
3172	28.761	28.26	438.56 (28.269)	4d(³ P)5p(⁴ P)6p ⁵ P ₁	5s _{1/2}	22.57 70 ^c	
3178	28.767		436.331 (28.413)	5s ² 8d ³ P ₁			
3193	28.777		436.166 (28.424)	4d(² P)(⁴ D)7s ³ D ₁			
3327	28.852	28.53	434.41 (28.539)	4d(² F)(⁴ F)7d ⁵ F ₁	5s _{1/2} 5p _{3/2}	22.84 71 ^c 19.76 30 ^b	
3364	28.873		431.530 (28.729)	5s ² 9s ³ P ₁			
3389	28.888		431.033 (28.762)	5s ² 8d ³ D ₁			
3421	28.908		430.168 (28.820)	4d(² F)(² D)7d ¹ P ₁			
3486	28.969		429.651 (28.855)	5s(¹ P)5p(² P)6p ³ D ₁			

^a Supposed satellite lines.^b Lines observed only by Schmitz *et al* [10].^c Lines observed only by Kazakov and Khristoforov [13].

assigned as those reflecting the autoionizing transitions (2) from the lowest states 258, 281, 523, 542, 606, 614. For all states with excitation energies higher than 26.9 eV (see state 1602 and above) the autoionizing transitions are not observed.

Multi-excited configurations. Double-excited and triple-excited configurations represent multi-electron transitions from the ground state 4p⁶5s² of Sr atoms. In the 4p⁵4d²5s lowest configuration, 29 autoionizing transitions (2) from 20

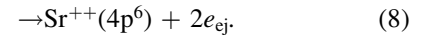
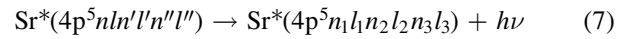
states, i.e., 117, 145, 154, 157, 159, 161, 162, 165, 168, 173, 176, 179, 185, 187, 188, 193, 199, 204, 210 and 233 are found in the present ejected-electron spectra. The preferable decay channels are transitions with formation of Sr^+ ions in the $5s_{1/2}$ and the $4d_{3/2}$ states. The comparison of the spectra in figures 1, 2 shows that the lines 62–69, 71, 72, which reflect the transitions into the $5s_{1/2}$ state, are the major contributors to the intensity of the spectra between 17.3 and 18.5 eV ejected-electron energy. All classified dipole-allowed states 154, 159, 173, 185, 199 and 210 are clearly seen also in the photoabsorption spectrum [8].

Of 38 states representing high-lying double-excited configurations $4p^5snln'l'$ only for 16 states, i.e., 133, 191, 264, 277, 288, 339, 373, 377, 379, 389, 478, 760, 1165, 1184, 1404 and 1493 the autoionizing transitions (2) are revealed in the electron spectra. The single-channel decay with formation of Sr^+ in the $5s_{1/2}$ ground state is a preferable decay mode for all states. For 11 states 428, 432, 507, 579, 631, 678, 1173, 1258, 1389, 1416, 1450 and 1482 located below 26.9 eV, and for six states 1512, 2129, 2229, 2415, 3156 and 3486 located above 26.9 eV, no autoionizing transitions (2) are observed. Note also that the complex structure of the photoabsorption spectra [8] in the energy range 19–20 eV required particular attention to the identification of the lines 75–77 which dominate in spectra at incident-electron energies $E_{\text{inc}} > 50$ eV (see figure 2). Their identification was performed only after the careful analysis of the photoabsorption spectra [8], the photoionization spectra [21], the *LSJ* assignments of levels (see section 4.2) and also taking into account the calculated values of the excitation cross sections, Auger yields and observed intensities of lines. In order to achieve full compliance between the calculated and the experimental energy spectra, the line 76 was considered consisting of three unresolved lines 76a, 76b, 76c that correspond to three maxima observed between 488 and 492 Å in the photoabsorption spectrum [8]. Also, the lines 24^b , 27^b reported by Schmitz *et al* [10] were included in the identification.

Of 17 states classified as belonging to the triple-excited configurations $4p^5nln'l'n''l''$ only four states 474, 2277, 3172, and 3327 reveal the autoionizing transitions (2) which are represented in spectra by the very weak ejected-electron lines 69^c – 71^c [13], 30^+ [10] and a satellite line $31'$. However, the relatively high excitation cross section predicted for these states (see table 1) is in contradiction with the low intensity of associated lines that indicates the existence for them of some additional decay channels. This situation requires some separate consideration.

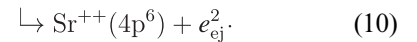
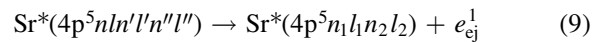
As follows from the analysis above and the results listed in table 2, of 54 classified atomic states possessing the radiationless decay mode (2) only three states 2277, 3178 and 3325 are located above the excitation threshold of the lowest ionic AIS ($4p^54d5s$) $^4P_{1/2}$ at 26.92 eV [11, 21]. For 19 states lying between 25.4 and 26.9 eV and for 21 states lying above 26.92 eV the autoionizing transitions into $4p^6nl$ ionic states were not revealed in ejected-electron spectra. And this despite the fact that their calculated autoionization probabilities are the same or even larger than for the low-lying AIS (see table 1). For the first group of 19 states (428, 447, 507, 523, 542, 562, 579, 631, 656, 678, 1173, 1198, 1258, 1278,

1389, 1416, 1450, 1474, 1482) the following decay channels are also possible



As our present calculations show, the radiative decay (7) is of low probability for all above states. This is confirmed also by the relatively broad profiles of the corresponding lines in photoexcitation spectra [8, 21]. The process (8) reflects Auger transitions with simultaneous ejection of two electrons. Being to some extent exotic, it is the only possible decay channel for the considered states. Due to the random nature of the energy distribution between two ejected-electrons, it can not be observed in the present ejected-electron spectra. However, its observation was reported earlier by detecting the Sr^{2+} yield in the energy region of the broad strong photoabsorption peak between 24.9 and 25.5 eV [21].

The absence of transitions (2) for the second group of 21 states lying above 26.92 eV is similar to the situation found earlier in Ba atoms [17] and explained by the presence of the two-step autoionization process [34]. For Sr atoms, it can be described by the following reactions



Accounting for process (9) in the present calculations significantly reduces the probability of the transitions from the high-lying states (from state 1512 above) into the $4p^6nl$ ionic states (see *B* values in brackets in table 1). This explains both low intensity of ejected-electron lines 69^c – 71^c and complete absence of transitions (2) for all 21 states located above 26.92 eV. The high efficiency of the process (9) at photon impact energies above 26.92 eV was shown also by photoionization studies [21]. The energies of ejected electrons e_{ej}^1 do not exceed 2 eV and, therefore, are out of the energy region studied in the present and all previous measurements while the ejected-electron lines reflecting the process (10) are clearly seen in the low-energy spectral region (see lines 13, 14, 16, 18–20 in spectra in figure 2).

5.2. Photoabsorption spectra

As was mentioned in section 4.2, the previous identification of lines in the photoabsorption spectrum of Sr atoms [8] was performed on the base of calculated excitation energies and oscillator strengths for the states with $J = 1$ from odd configurations obtained in the configuration-interaction approximation using the basis of numerical solutions of Hartree–Fock equations in quasi-relativistic approach and by scaling down *ab initio* Slater–Condon parameters. Eighty-one lines not included in Rydberg series were identified as excitations of the states in single-excited $4p^55s^24d, 6s$, double-excited $4p^54d^25s$, $4p^55s5p^2$ and triple-excited $4p^54d^3$, $4p^54d5p^2$ configurations. Also, 55 lines mainly from the long-wave part of the spectrum were associated with ejected-electron lines observed by White *et al* [11].

The full set of excitation and decay parameters of the $4p^5nln'l'n''l''$ states obtained in the present work using the large-scale configuration-interaction method in the basis of

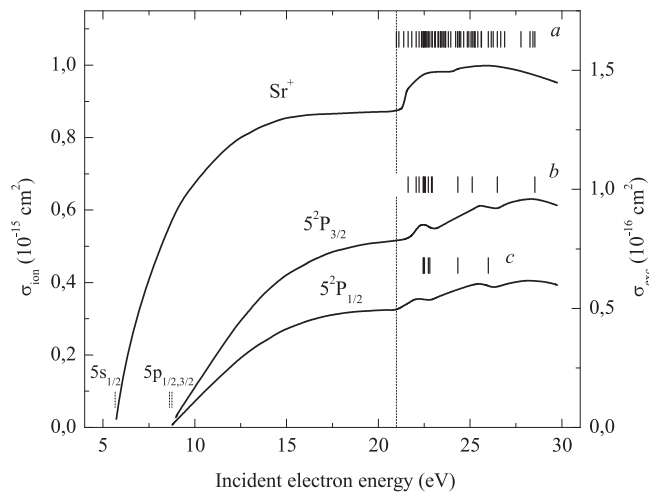


Figure 3. Ionization cross section σ_{ion} [36] of Sr atoms and excitation cross sections σ_{exc} of $\text{Sr}^+ 5^2\text{P}_{1/2,3/2}$ levels [37] from the ground state of SrI. Excitation thresholds for classified AIS (see table 2) are marked by bars. The vertical dash lines indicate the 5^2S ionization threshold at 5.695 eV [6], the excitation thresholds of the $\text{Sr}^+ 5^2\text{P}_{1/2,3/2}$ levels at 8.635 and 8.735 eV [6] as well as the excitation threshold of the 4p^6 subshell at 20.98 eV (present data).

the solutions of Dirac–Fock–Slater equations made it possible to carefully analyze and compare the intensity distributions in ejected-electron and photoabsorption spectra, the widths of observed photoabsorption lines and, therefore, to reconsider their earlier classification. All photoabsorption lines with a non-zero width and a strength lying between 587.5 and 429.7 Å are identified and listed in table 2. As can be seen, the excitation of the $4\text{d}5\text{s}^2\ ^3\text{P}_1$ state (104) gives rise to the 4p -subshell photoabsorption spectrum of Sr atoms. The vast part of the states with $J = 1$ (49 of 68) associated with photoabsorption lines are from double-excited odd configurations. It is also shown that the broad and strong photoabsorption peak at 490.92 Å assigned erroneously in [8] as the non-existent in reality $^1\text{P}_1$ level from the $5\text{p}^5\text{d}6\text{s}^2$ configuration is actually a superposition of at least three lines at 491.84, 490.92 and 489.750 Å which reflect the excitation of three states 373, 377 and 379 from different double-excited configurations. The fact that only a half of the total number of classified states is found in the photoabsorption spectra once again showed the high efficiency of using an electron impact of regulated energy for studying the excitation behavior of dipole-forbidden atomic states.

The performed identification of the lines in ejected-electron and photoabsorption spectra makes now clear the origin of the well-known structures observed in the experimental ionization cross section σ_{ion} [35, 36] and in the excitation cross sections σ_{exc} of $\text{Sr}^+ 4\text{p}^6nl$ levels [37]. Indeed, as can be seen from figure 3, the rise of the ionization cross section just above the excitation threshold of the 4p^6 subshell reflects the overall contribution of the autoionizing transitions from the whole set of the states $4\text{p}^5nl'n''l''$ located between 21 and 28 eV (see level group *a*). The lowest and most effectively excited configurations $4\text{p}^54\text{d}5\text{s}^2$, $4\text{p}^55\text{s}^25\text{p}$, $4\text{p}^54\text{d}^25\text{s}$, and $4\text{p}^54\text{d}5\text{s}5\text{p}$ would play the crucial role in this process. The maxima observed in the excitation functions of the $5^2\text{P}_{1/2}$ and $5^2\text{P}_{3/2}$ ionic levels reflect their cascade

population by the autoionizing transitions from two group of atomic AIS, namely 105, 107, 138, 377, and 606 (level group *c*) and 103, 106, 110, 133, 143, 156, 223, 339, 377, 447, and 1184 (level group *b*). The resonant shape of the first maxima points out the resonant excitation character of the lowest AIS 104–107 and 110 at the near-threshold impact energies.

6. Summary

The ejected-electron spectra of strontium atom were measured in a broad incident-electron impact energy range. The excitation energies and intensity behaviors were investigated for 58 lines observed between 12 and 21 eV ejected-electron kinetic energy. These data together with the results of the *ab initio* calculations on excitation energies, cross sections and branching ratios of 105 states in the $4\text{p}^5nl'n''l''$ ($nl = 4\text{d}, 5\text{s}, 5\text{p}; n''l'' = 4\text{d}, 5\text{s}, 5\text{p}; n''l'' = 5\text{s}, 6\text{s}, 7\text{s}, 8\text{s}, 9\text{s}, 5\text{p}, 6\text{p}, 5\text{d}, 6\text{d}, 7\text{d}, 8\text{d}, 4\text{f}, 5\text{g}$) configurations were used for accurate and detailed spectroscopic assignment of 60 lines in ejected-electron spectra and 68 lines in photoabsorption spectra.

The lowest and most effectively excited configurations $4\text{p}^54\text{d}5\text{s}^2$, $4\text{p}^55\text{s}^25\text{p}$, $4\text{p}^54\text{d}^25\text{s}$, and $4\text{p}^54\text{d}5\text{s}5\text{p}$, 6s play the leading role in excitation-autoionization processes in Sr atoms below the ionization threshold of the 4p^6 subshell at 26.92 eV. Most of the states in these configurations possess two and three decay channels with formation of Sr^+ in the $5\text{s}_{1/2}$, $4\text{d}_{3/2,5/2}$ and $5\text{p}_{1/2,3/2}$ states.

For 19 states with excitation thresholds between 25.4 and 26.9 eV and for 21 states with excitation thresholds above 26.9 eV, the autoionizing transitions into the 4p^6nl ionic states were not revealed in ejected-electron spectra. Instead, two-electron Auger transitions and two-step autoionization are proposed for these states as the main decay processes resulted in formation of Sr^{2+} in the $4\text{p}^6\ ^1\text{S}_0$ ground state.

Acknowledgments

The authors wish to thank Dr O Zatsarinny for transformation of the expansion coefficients from *jjj* to *LSJ* coupling scheme. This work was funded by the National Academy of Sciences of Ukraine through projects # 0112U002079 and 0117U003239.

ORCID iDs

A Kupliauskienė <https://orcid.org/0000-0002-3493-4886>

A Borovik <https://orcid.org/0000-0002-3111-2932>

References

- [1] Killiana T C, Pattard T, Pohl T and Rost J M 2007 *Phys. Rep.* **449** 77
- [2] Calegari F, Sansone G, Stagira S, Vozzi C and Nisoli M 2016 *J. Phys. B: At. Mol. Opt. Phys.* **49** 062001
- [3] Lemonde P 2009 *Eur. Phys. J. Spec. Top.* **172** 81

- [4] Gorshkov A V, Rey A M, Daley A J, Boyd M M, Ye J, Zoller P and Lukin M D 2009 *Phys. Rev. Lett.* **102** 110503
- [5] Courtillot I, Quessada-Vial A, Brusch A, Kolker D, Rovera G D and Lemonde P 2005 *Eur. Phys. J. D* **33** 161
- [6] Kramida A, Ralchenko Y, Reader J and (NIST ASD Team) 2015 *NIST Atomic Spectra Database (ver. 5.3)* (Gaithersburg, MD: National Institute of Standards and Technology)
- [7] Mansfield M W D and Connerade J P 1975 *Proc. R. Soc. A* **342** 421
- [8] Mansfield M W D and Newsom G H 1981 *Proc. R. Soc. A* **377** 431
- [9] Connerade J P, Baig M A and Sweeney M 1990 *J. Phys. B: At. Mol. Opt. Phys.* **23** 713
- [10] Schmitz W, Breuckmann B and Mehlhorn W 1976 *J. Phys. B: At. Mol. Phys.* **9** L493
- [11] White M D, Rassi D and Ross K J 1979 *J. Phys. B: At. Mol. Phys.* **12** 315
- [12] Borovik A A, Aleksakhin I S, Bratsev V F and Kuplyauskene A V 1982 *Opt. Spectrosk.* **53** 976 in Russian
- [13] Kazakov S M and Khristoforov O V 1985 *Sov. Phys.—JETP* **61** 656
- [14] Borovik A, Vakula V and Kupliauskienė A 2007 *Lith. J. Phys.* **47** 129
- [15] Kupliauskienė A and Kerevičius G 2013 *Phys. Scr.* **88** 065305
- [16] Borovik A, Kupliauskiene A and Zatsarinny O 2011 *J. Phys. B: At. Mol. Opt. Phys.* **44** 145203
- [17] Hrytsko V, Kerevičius G, Kupliauskienė A and Borovik A 2016 *J. Phys. B: At. Mol. Opt. Phys.* **49** 145201
- [18] Gu F M 2008 *Can. J. Phys.* **86** 675
- [19] Borovik A A, Grum-Grzhimailo A N, Bartschat K and Zatsarinny O 2005 *J. Phys. B: At. Mol. Opt. Phys.* **38** 1081
- [20] Nesmejanov A N 1963 *Vapor Pressure of the Elements* (New York: Academic)
- [21] Nagata T et al 1986 *J. Phys. B: At. Mol. Phys.* **19** 1281
- [22] Balashov V V, Lipovetskii S S and Senashenko V S 1973 *Sov. Phys.—JETP* **36** 858
- [23] Kuchiev M Y and Sheinerman S A 1988 *J. Phys. B: At. Mol. Opt. Phys.* **21** 2027
- [24] Kupliauskienė A 2004 *Lith. J. Phys.* **44** 199
- [25] Kupliauskienė A 2007 *Phys. Scr.* **75** 524
- [26] Kupliauskienė A and Tutlys V 2009 *Nucl. Instrum. Methods* **267** 263
- [27] Kupliauskienė A and Tutlys V 2003 *Phys. Scr.* **67** 290
- [28] Haq S-ul, Mahmood S, Amin N, Jamil Y, Ali R and Baig M A 2006 *J. Phys. B: At. Mol. Opt. Phys.* **39** 1587
- [29] Hudson R D, Carter V L and Young P A 1969 *Phys. Rev.* **180** 77
- [30] Chu C C, Fung H S, Wu H H and Yih T S 1998 *J. Phys. B: At. Mol. Opt. Phys.* **31** 3843
- [31] Aleksakhin I S, Bogachev G G, Zapesochnyi I P and Ugrin S Y 1981 *Sov. Phys.—JETP* **53** 1140
- [32] Pejčev V and Ross K J 1977 *J. Phys. B: At. Mol. Phys.* **10** 2935
- [33] Cowan R D 1981 *Theory of Atomic Spectra* (Berkeley, CA: University of California Press)
- [34] Hotop H and Mahr D 1975 *J. Phys. B: At. Mol. Phys.* **8** L301
- [35] Okuno Y 1971 *J. Phys. Soc. Japan* **31** 1189
- [36] Vainshtein L A, Ochkur V I, Rakhovskii V I and Stepanov A M 1972 *Sov. Phys.—JETP* **34** 271
- [37] Chen S T, Leep D and Gallagher A 1976 *Phys. Rev. A* **13** 947